Scripta Materialia 238 (2024) 115754

Contents lists available at ScienceDirect

Scripta Materialia

journal homepage: www.journals.elsevier.com/scripta-materialia

Facile and fast synthesis of highly ordered $L1_0$-FeNi nanoparticles

G. Varvaro [a,*], P. Imperatori [a], S. Laureti [a], D. Peddis [b,a], F. Locardi [b], M. Ferretti [b], C. Cannas [c], M. Sanna Angotzi [c], N. Yaacoub [d], A. Capobianchi [a,*]

[a] CNR, Istituto di Struttura della Materia, nM²-Lab, Monterotondo Scalo (Roma), 00015, Italy
[b] Università degli Studi di Genova, Dipartimento di Chimica e Chimica Industriale, nM²-Lab, Via Dodecaneso 31, 1-16146 Genova, Italy
[c] Università di Cagliari and INSTM, Dipartimento di Scienze Chimiche e Geologiche, S.S. 554, bivio per Sestu, 09042, Monserrato, Italy
[d] Le Mans Université, Institut des Molécules et Matériaux du Mans, CNRS UMR-6283, Avenue Olivier Messiaen, Le Mans, 72085, France

ARTICLE INFO

Keywords:
$L1_0$ FeNi
Preordered precursor reduction
Nanoparticles
Permanent magnets

ABSTRACT

The chemically ordered $L1_0$-FeNi alloy is a promising candidate for next generation rare-earth-free permanent magnets, which can revolutionize the high-performance magnets market currently dominated by Nd-Fe-B. Despite many efforts, the experimental results fall short of theoretical predictions, and current approaches are not suitable for industrial implementation. In this work, we propose an innovative and efficient synthesis method that exploits the natural order of a crystalline Ni/Fe complex, which closely mimics the atomic organization in the $L1_0$ structure, to drive the formation of the ordered phase. By low-temperature reduction of the complex salt, carbon coated aggregates of FeNi alloy nanoparticles (20 – 120 nm) with a >55% of $L1_0$ phase, high coercivity (up to 65 mT) and large saturation magnetization (~ 140 Am^2/kg) were obtained. The results pave the way for the development of a novel and sustainable route to produce high-anisotropy FeNi nanoparticles of potential interest for next generation critical-element-free permanent magnets.

Permanent magnets are fundamental components in a wide variety of primary applications ranging from energy-conversion devices, household appliances, to rapidly developing green technologies (i.e., hybrid vehicles, wind turbines) [1]. Current high-performance permanent magnets owe their extraordinary properties to the presence of rare-earth elements (REEs), which allows reaching a maximum energy product $(BH)_{max}$ as high as 0.5 MJ/m^3 at room temperature in Nd-Fe-B compounds [2]. However, the supply of REEs is nowadays a critical issue for the permanent magnet industry. Indeed, the extremely low number of extraction sites (> 80% of the global supply of refined REEs come from China), combined with their continuously growing demand, makes the REEs extremely vulnerable to price fluctuations and shortage [2]. Moreover, the mining and refining processes of REEs require large amounts of energy and water, while generating vast volumes of GHG emissions [3]. To alleviate the strong environmental and economic impact of the RE industry, an intense computational and experimental activity has been carried out to develop effective solutions that allow reducing the demand of REEs, including the optimization of existing materials and magnets' design [2,4–11], the development of new hard magnetic phases [12,13], and the recycling/reuse of End-of-Life magnets [14–17]. Although there is still room for improving the performance of conventional materials, a major achievement would be to develop new hard magnetic phases based on non-critical, easily accessible and reusable/recyclable elements (e.g., Fe, Ni, Mn, Al) [18] capable of matching the performance of the state-of-art RE-based permanent magnets, or bridging the gap in terms of cost-performance [10] between the cheapest but less performing hexaferrites ($(BH)_{max}$ up to ~45 kJ/m^3 at room temperature) and the RE-based permanent magnets [4]. Several materials have been investigated for this purpose [12], and, among them, the chemically ordered $L1_0$ FeNi equiatomic alloy (*tetrataenite*), consisting of planes of Fe and Ni atoms alternating along the *c*-axis of the tetragonal *fct* unit cell, has attracted a great deal of attention owing to the low-cost and safe supply of their constituent elements along with the large energy product, which may ideally reach values as large as ~0.45 MJ/m^3 [19]. Moreover, the FeNi alloy, with its lower Fe content compared to Nd-Fe-B magnets and a reduced water and energy usage related to the mining and processing of Ni in comparison to rare-earth elements [20], is expected to result in a decreased overall energy and environmental impact. However, differently to other hard $L1_0$ alloys, such as FePt(Pd) and CoPt(Pd), which can be obtained by conventional thermal processes [21–26], the fabrication of the $L1_0$-FeNi phase is extremely challenging due to the low chemical order/disorder

* Corresponding authors.
E-mail addresses: gaspare.varvaro@ism.cnr.it (G. Varvaro), aldo.capobianchi@ism.cnr.it (A. Capobianchi).

https://doi.org/10.1016/j.scriptamat.2023.115754
Received 10 May 2023; Received in revised form 8 August 2023; Accepted 4 September 2023
Available online 15 September 2023

transition temperature ($T_{O\text{-}D} \approx 320$ °C) [27] above which a chemically disordered cubic *fcc* (A1) phase with soft magnetic properties forms. Indeed, although the $L1_0$ phase is stable at low temperature, to promote the chemical ordering, the processing temperature needs to be lower than $T_{O\text{-}D}$ but high enough to ensure an adequate atomic interdiffusion [28]. Due to the low $T_{O\text{-}D}$ value of the FeNi alloy, the low atomic mobility below $T_{O\text{-}D}$ kinetically limits the formation of the $L1_0$ phase, which is indeed naturally found only in meteorites that have cooled through billions of years at extremely low cooling rates (1 K per million years) [29]. To favor the formation of the ordered phase under easily accessible conditions and time scales, several strategies have been proposed [19], including neutron irradiation [30], oxidation and reduction cycles [31], rapidly solidification of glassy alloys [32], alternate deposition of Fe end Ni monoatomic layers in thin films [33,34], nitrogen insertion and topotactic extraction (NITE) [35], addition of other elements [36], the exploitation of plastic deformation [37] or epitaxial strains induced by suitable templates [38,39] as well as the application of simultaneous stress and magnetic field during prolonged thermal treatments [40]. Although promising results were obtained in some cases, none of the proposed approaches is demonstrated to guarantee the production of the $L1_0$-FeNi alloy with levels of performance, yield, times, costs, and environmental sustainability that can be used to produce the material at the industrial scale. As an example, the NITE process [35], which allows so far achieving the best results in terms of phase purity and magnetic hardness, is rather complex and expensive as it involves multiple thermal treatments (up to 300 °C and 50 h) in significantly high flows of hydrogen (1 L/min) and ammonia (5 L/min) for the processing of only one gram of product, effectively limiting its use for a low-cost massive production of FeNi-based permanent magnets.

To overcome the limitations of previously proposed approaches for synthesizing the $L1_0$-FeNi alloy, we used an effective and easily scaled-up synthesis method (*Preordered Precursor Reduction*) developed by the authors of the present work to synthesize MPt (M = Fe, Co, Ni) $L1_0$ alloys, which allows reducing the energy required to order the metallic atoms by exploiting the natural order of crystalline precursor salts [28, 41–46]. To obtain the FeNi alloy, a crystalline *Nickel Nitroprusside* complex, $NiFe(CN)_5NO{\bullet}xH_2O$, containing Fe and Ni atoms with a 1:1 ratio arranged on alternating planes resembling the structure of the $L1_0$ alloy (Fig. 1), was used as precursor to drive the formation of the $L1_0$ phase by low-temperature treatments in a reductive atmosphere. Differently to conventional approaches where thermal processes are exploited to induce the disorder/order transition, the proposed strategy, for which a patent application was recently filed [47], is based on the opposite paradigm, that is the preservation during the thermal treatment of the chemical order provided by the crystal.

Crystals of *Nickel Nitroprusside*, $NiFe(CN)_5NO{\bullet}xH_2O$, were thermal treated in H_2 atmosphere for different reaction times ($12 < t < 72$ h) and processing temperatures ($250 < T_p < 450$ °C); the resulting powders were then analysed for their structural, morphological and magnetic properties (details are shown in *Supplementary Materials*). In the following, the properties of two representative samples obtained at $T_p = 290$ °C (S290) and $T_p = 400$ °C (S400), i.e., at processing temperatures either slightly lower or higher than $T_{O\text{-}D}$, respectively, are discussed to demonstrate the feasibility and the effectiveness of the proposed synthesis method. The samples were obtained after a treatment of 24 h, as no further improvements of the magnetic properties were observed for longer reaction times (Fig. S1a and c, *Supplementary Materials*).

The main results of the structural and microstructural analysis of samples S290 and S400 are summarized in Fig. 2. Both the samples show an XRD pattern (Fig. 2a and b) that is characteristic of the FeNi metal alloy. Other phases, such as Fe/Ni oxides (e.g., NiO or Fe_2O_3, Fe_3O_4), which would affect, if present, the magnetic properties of the material, were not detected (see Fig. S2 in *Supplementary Materials* for an XRD logarithmic plot). A univocal attribution of the reflections to the tetragonal or to the cubic phase is not possible by using a conventional X-ray source, as in our case. This is because of the small difference between Fe and Ni X-ray scattering factors, resulting in extremely weak superlattice reflections (originating from the alternate stacking of Fe and Ni planes along the *c* direction), which assume a maximum value of 0.3% of that of the fundamental (111) peak for the case of the strongest superlattice (001) reflection at $2\theta \approx 25°$. In addition, the slight difference between the lattice parameters of the two phases ($a_{fcc} = 3.603$ Å; $a_{fct} = b_{fct} = 3.582$ Å and $c_{fct} = 3.607$ Å [48]), with a c/a ratio in the tetragonal structure very close to 1, leads to a tiny splitting of fundamental peaks. Furthermore, as shown from the Mössbauer results reported below, only a fraction of the $L1_0$ phase is present, further reducing the intensity of superstructure reflections. From the Rietveld fit of the XRD data, an average crystallite size of 24 ± 1 and 83 ± 2 nm was derived for samples S290 and S400, respectively, thus suggesting an increase of the powder's crystallinity induced by the higher processing temperature. Regarding the morphology, TEM analysis of sample S290 (Fig. 2c and d) indicates that the FeNi powders consists of micrometer-size aggregates of nanoparticles ranging in between 20 and 120 nm. A deeper inspection shows that most of the particles are rounded (white dashed circles) with a mean size of 40 – 50 nm, while a minority fraction consists of spherical particles with sizes in the 20 to 40 nm range and few larger particles that rarely reach 120 nm. Moreover, the images show that the particles' aggregates are surrounded by a 3 – 7 nm thick carbon shell (Fig. 2d) originating from the precursor. Increasing the processing temperature (S400), does not lead to a significant change of the morphology that still consists of micrometer-size aggregates of nanoparticles coated by a thin carbon shell (Fig. 2e and f). TEM-EDX analysis (Fig. S3a) on different areas of the samples confirms that the nominal 1:1 stoichiometry of the alloy is maintained both considering point and selected area measurements. This is also proved by the homogeneous distribution of Ni and Fe all over the particles as shown in the elemental mappings reported in Fig. S3b and the almost perfect overlapping of Ni and Fe composition profile along a line (Fig. S3c and d). Apart from Fe, Ni and C, TEM-EDX analysis shows the presence of a very small amount of Na and O impurifies (from 1 to 3 in atomic%), likely deriving from the synthesis of Nickel Nitroprusside (see

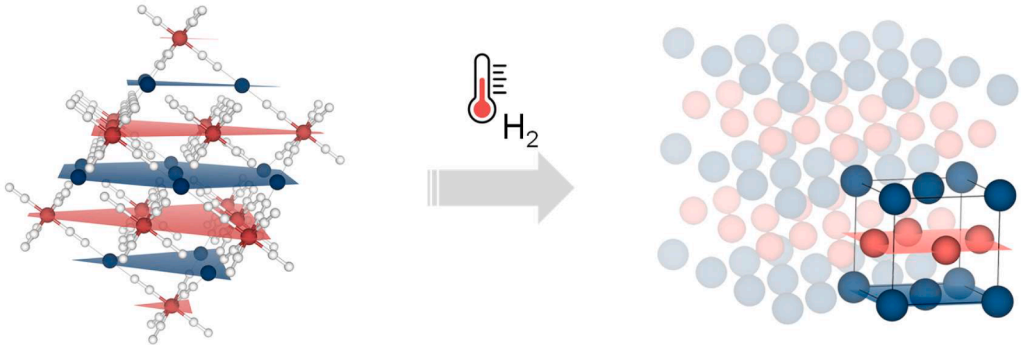

Fig. 1. Schematic representation of the synthesis process. Crystals of *Nickel Nitroprusside*, $NiFe(CN)_5NO{\bullet}xH_2O$, are used as precursors to obtain $L1_0$-FeNi nanoparticles by low-temperature reduction in H_2 atmosphere. For clarity of representation, only the metal atoms (Fe in red and Ni in blue) are highlighted in the crystallographic structure of the precursor complex, while all the other elements (C, N, O, H) are shown in white. Fe and Ni atoms lie on alternating planes highlighted in red (Fe) and blue (Ni) resembling the atomic arrangement of the $L1_0$ FeNi structure.

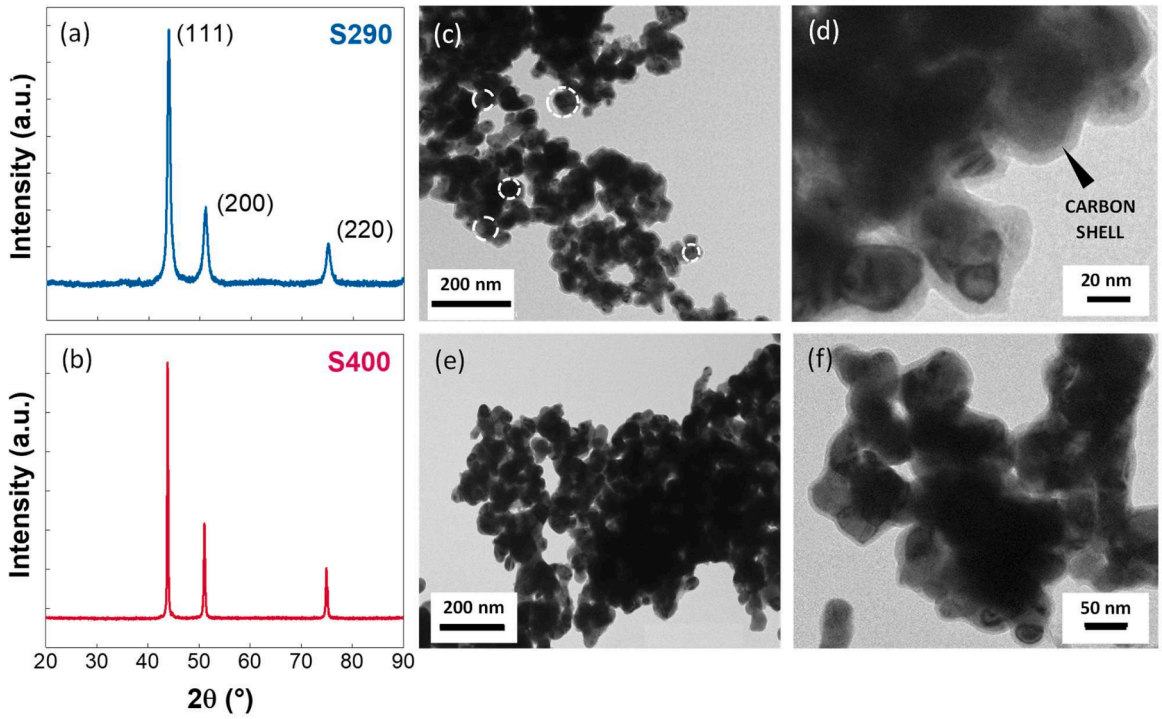

Fig. 2. (a, b) XRD patterns of samples (a) S290 and (b) S2400. (c – f) TEM images at different magnifications of samples (c, d) S290 and (e, f) S400.

Materials and Methods, *Supplementary Materials*), which does not affect the final properties of the powder.

Although the samples present similar structural and morphological properties, the magnetic behavior is clearly different as shown in Fig. 3, reporting on the field-dependent magnetic loops measured at 25 °C. Both the samples present a high saturation magnetization (~140 Am^2/Kg), which is slightly lower than the bulk value (154 Am^2/Kg), likely because of the presence of the non-magnetic carbon shell originating from the precursor complex. On the other hand, a significant variation of the coercive field is observed as the experimental conditions change. At $T_p < T_{O\text{-}D}$ the coercivity assumes a rather high value ($\mu_0 H_c \approx 56$ mT), which is not compatible with the A1 phase of the FeNi alloy; when the processing temperature is increased above $T_{O\text{-}D}$, the coercivity significantly reduces to ~19 mT.

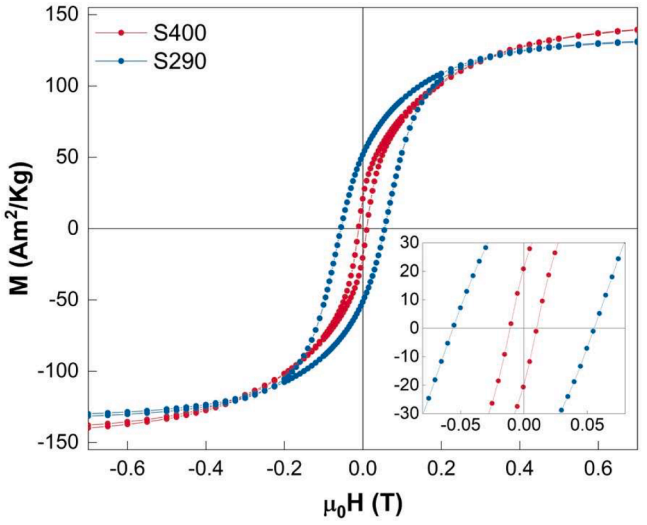

Fig. 3. Field-dependent magnetization loops of samples S290 and S400 measured at 25 °C. In the inset, a magnification around the coercive fields is reported.

To reveal the source of such pronounced difference in magnetic performance between the two samples, Mössbauer spectroscopy was performed at room temperature. This technique is indeed sensitive to the local neighborhood of Fe, which varies according to the chemical order of the alloy, thus allowing identifying the presence of the $L1_0$ phase [49]. The spectra (Fig. 4a and c) consist of six broad and asymmetrical lines and a singlet in low percentage. Due to the asymmetry of the lines, the spectra cannot be modelled neither using one singlet and one sextet with broad lines nor one singlet and one hyperfine magnetic field distribution (HMFD). Then, for a correct fit of the spectra, another approach is proposed, involving two HMFDs and one singlet corresponding to two ferromagnetic phases and a paramagnetic one, respectively. Consequently, the magnetic hyperfine structure was divided into two independent components associated with HMFD and different values of isomer shifts to describe the asymmetry of the lines. The HMFDs estimated from the proposed model are shown in Fig. 4b and d. Two principal domains were observed and associated to the ferromagnetic sub-spectra: the high-field component (mean value: 32.5 – 33 T) can be attributed to the A1 phase, while the low field component (mean value: 29.5 – 30 T) can be ascribed to the $L1_0$ phase [49] (Table S1, *Supplementary Materials*). The analysis of the Mössbauer spectra clearly indicates the presence of both phases in the two samples. The estimation of the percentage of the $L1_0$ phase is roughly determined, because of the overlapping, by the area underlying the distribution of the hyperfine magnetic fields. This percentage is maximum in the case of the S290 sample (~58%), which also has the highest coercive field value, and decreases to ~33% in the S400 sample, thus resulting in a lower coercivity related to the increase of the cubic A1 phase percentage, whose formation is thermodynamically favoured at $T_p > T_{O\text{-}D}$. A deeper insight into the effect of the processing temperature shows that the coercivity reduces with the increase of the temperature in a way that resembles the reduction of the $L1_0$ content (Fig. 5). Such a striking parallelism strongly suggests that the coercivity evolution is primarily driven by a change in the intrinsic magnetic anisotropy resulting from the formation of the $L1_0$ phase. Slightly differences in the samples' morphology (e.g., size of particles/aggregates, density of local defects, etc.), are likely to have a

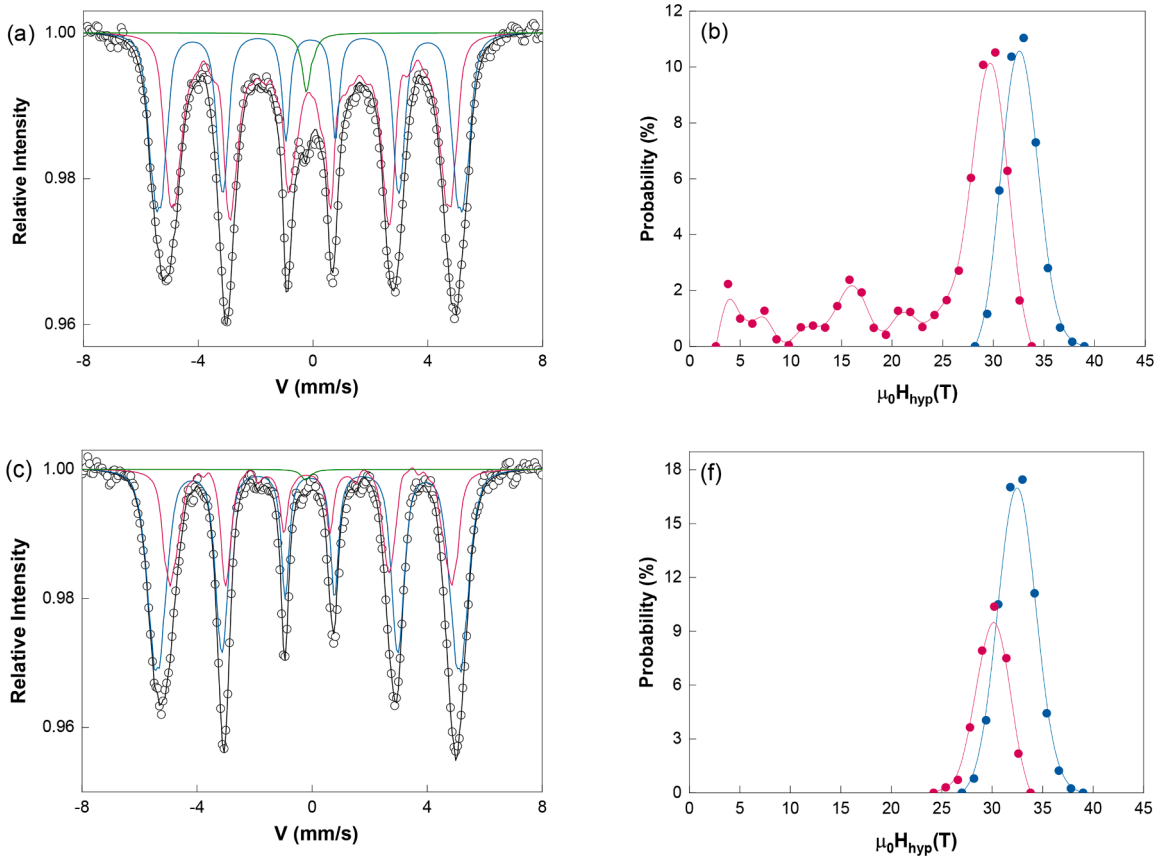

Fig. 4. (a,c) Mössbauer spectra of samples (a) S290 and (c) S400 collected at 25 °C. The experimental data are shown by the white dots and the fittings are shown by continuous lines on the measured data. The individual sub-spectra forming the fitting line are indicated by blue/red (ferromagnetic components) and green (paramagnetic component) lines. (b,d) Hyperfine magnetic field distribution (HMFD) of the two sub-spectra corresponding to the ferromagnetic components of samples (b) S290 and (d) S400.

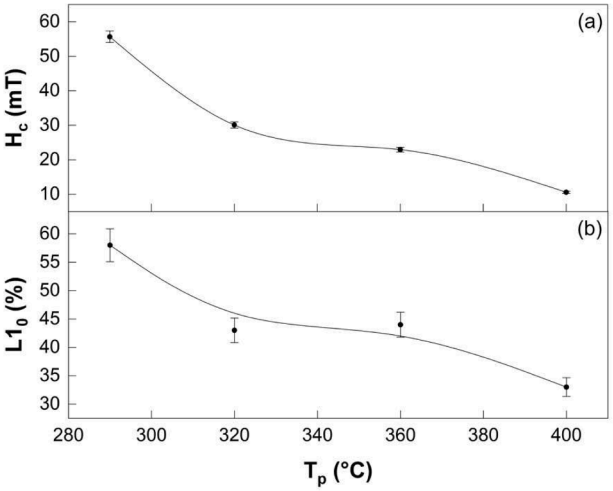

Fig. 5. Evolution of the (a) coercivity and (b) $L1_0$ content, as obtained from the fitting of the Mössbauer spectra, as a function of the processing temperature (T_p). The field-dependent magnetization loop and the Mössbauer spectra of samples synthesized at 320 °C and 360 °C (t = 24 h) are reported in Figs. S1d and S4 (*Supplementary materials*), respectively.

minor influence.

The formation of the $L1_0$ phase is further substantiated by two additional experimental findings. First, the direct current demagnetization (DCD) curve of sample S290 (Fig. S5, *Supplementary Materials*), a measurement sensitive only to irreversible processes, shows a remanence coercivity (~80 mT) that is 40% higher than the coercivity (~56 mT). This implies the presence of reversible processes, likely connected to very small isolated particles that are superparamagnetic at room temperature; indeed, the limiting diameter for the transition to the superparamagnetic regime (at room temperature and in a standard time measurement of about 100 s) [50,51] can be approximated to ~10 nm for the $L1_0$ phase ($K \sim 5 \times 10^5$ J/m^3) and ~45 nm for the A1 phase ($K \sim 0.6 \times 10^5$ J/m^3) [52]. Their presence suppresses the coercive field, which could potentially increase up to ~80 mT by controlling particle size. Moreover, by treating the S290 sample with a 0.1 M HCl solution, which preferentially dissolves the chemically disordered phase [48], results in an enhancement of the coercivity up to ~65 mT (Fig. S6, *Supplementary Materials*), which may be ascribed to the increase of the $L1_0$ phase percentage.

The combined analysis of the field-dependent magnetization loops and the Mössbauer spectra demonstrates that the initial order of the crystalline complex favors the formation of the ordered phase that is maximum in percentage when the processing temperature is slightly lower than the order/disordered transition temperature. When $T_p > T_{O-D}$, the thermodynamics of the process tends to favor the formation of the disordered phase by contrasting the initial order of the crystalline complex with a consequent reduction in the percentage of the $L1_0$ phase and, consequently, of the coercivity.

In summary, we developed a novel and efficient strategy, which allows synthesizing highly ordered $L1_0$-FeNi powders under much more favorable conditions compared to other approaches. The method exploits the natural order of a crystalline Nickel Nitroprusside complex, resembling the atomic arrangement of the $L1_0$ structure, to drive the

formation in a reasonable time (< 24 h) of the ordered FeNi phase by simple low temperature reduction (< 300 °C) of the precursor complex in a low hydrogen flow (0.01 L/min at steady state). By properly adjusting the experimental conditions, carbon coated (2–7 nm) aggregates of FeNi alloy nanoparticles (20 – 120 nm) with a >55% of $L1_0$ phase, high coercivity (up to 65 mT) and large saturation magnetization (~ 140 Am^2/kg, close to the bulk value) were obtained. Despite the rather high percentage of chemically ordered phase that was obtained, the coercivity is not yet optimal for a high-performance permanent magnet, likely because of a not perfect chemical order of the $L1_0$ phase [53] and/or the specific morphology of the sample consisting of micrometer-size aggregates of nanoparticles. Although further actions are necessary to enhance the fraction of the ordered phase and improve the overall magnetic properties, the results clearly prove the effectiveness and high potential of the developed strategy, which can also be extended to other complexes with a 1:1 Fe/Ni ratio (e.g., $Fe(H_2O)_2Ni(CN)_4$) [47]. The results of our study lay the groundwork for pioneering a novel and efficient chemical synthesis methodology to obtain high-anisotropy FeNi nanoparticles. With further refinement, these nanoparticles may serve as the components for manufacturing next-generation permanent magnets free of critical raw materials. However, substantial optimization of post-synthesis processes remains imperative before these materials can be used for this purpose. For instance, consolidation methods must be developed to assemble the nanoparticles into dense compacts while retaining the magnetic properties of the constituent materials. Additionally, techniques to tailor and control the alignment of the nanoparticles' easy axes of magnetization relative to the macroscopic geometry must be developed. Overcoming these processing challenges will be essential to fully capitalize on the unique our strategy for manufacturing critical-element-free permanent magnets.

CRediT authorship contribution statement

G. Varvaro: Conceptualization, Supervision, Writing – original draft, Writing – review & editing. **P. Imperatori:** Investigation, Formal analysis, Writing – review & editing. **S. Laureti:** Investigation, Formal analysis, Writing – review & editing. **D. Peddis:** Investigation, Formal analysis, Writing – review & editing. **F. Locardi:** Investigation, Formal analysis, Writing – review & editing. **M. Ferretti:** Investigation, Formal analysis, Writing – review & editing. **C. Cannas:** Investigation, Formal analysis, Writing – review & editing. **M. Sanna Angotzi:** Investigation, Formal analysis, Writing – review & editing. **N. Yaacoub:** Investigation, Formal analysis, Writing – review & editing. **A. Capobianchi:** Conceptualization, Supervision, Methodology, Writing – review & editing.

Declaration of Competing Interest

The authors declare that they have no known competing financial interests or personal relationships that could have appeared to influence the work reported in this paper.

Acknowledgments

The authors acknowledge the technical support provided by Enrico Patrizi for the magnetic characterization of the samples and "Centro Servizi di Ateneo per la Ricerca (CeSAR)" for the use of the TEM measurements performed with JEOL JEM 1400 PLUS.

Supplementary materials

Supplementary material associated with this article can be found, in the online version, at doi:10.1016/j.scriptamat.2023.115754.

References

[1] O. Gutfleisch, M.A. Willard, E. Brück, C.H. Chen, S.G. Sankar, J.P. Liu, Magnetic materials and devices for the 21st century: stronger, lighter, and more energy efficient, Adv. Mater. 23 (2011) 821–842.
[2] J.M.D. Coey, Perspective and prospects for rare earth permanent magnets, Engineering 6 (2020) 119–131.
[3] S.R. Golroudbary, I. Makarava, A. Kraslawski, E. Repo, Global environmental cost of using rare earth elements in green energy technologies, Sci. Total Environ. 832 (2022), 155022.
[4] C. De Julián Fernández, C. Sangregorio, J. de la Figuera, B. Belec, D. Makovec, A. Quesada, Progress and prospects of hard hexaferrites for permanent magnet applications, J. Phys. D. Appl. Phys. 54 (2021), 153001.
[5] A. Kovacs, J. Fischbacher, M. Gusenbauer, H. Oezelt, H.C. Herper, O.Y. Vekilova, P. Nieves, S. Arapan, T. Schrefl, Computational design of rare-earth reduced permanent magnets, Engineering 6 (2020) 148–153.
[6] H. Nakamura, The current and future status of rare earth permanent magnets, Scr. Mater. 154 (2018) 273–276.
[7] R.L. Stamps, S. Breitkreutz, J. Åkerman, A.V. Chumak, Y. Otani, G.E.W. Bauer, J. U. Thiele, M. Bowen, S.A. Majetich, M. Kläui, I.L. Prejbeanu, B. Dieny, N. M. Dempsey, B. Hillebrands, The 2014 magnetism roadmap, J. Phys. D. Appl. Phys. 47 (2014), 333001.
[8] B. Balamurugan, D.J. Sellmyer, G.C. Hadjipanayis, R. Skomski, Prospects for nanoparticle-based permanent magnets, Scr. Mater. 67 (2012) 542–547.
[9] P. Maltoni, T. Sarkar, G. Varvaro, G. Barucca, S.A. Ivanov, D. Peddis, R. Mathieu, Towards bi-magnetic nanocomposites as permanent magnets through the optimization of the synthesis and magnetic properties of $SrFe_{12}O_{19}$ nanocrystallites, J. Phys. D. Appl. Phys. 54 (1–10) (2021), 124004.
[10] J.M.D. Coey, Permanent magnets: plugging the gap, Scr. Mater. 67 (2012) 524–529.
[11] H. Tahanian, M. Aliahmadi, J. Faiz, Ferrite permanent magnets in electrical machines: opportunities and challenges of a non-rare-earth alternative, IEEE Trans. Magn. 56 (2020), 900120.
[12] J. Cui, M. Kramer, L. Zhou, F. Liu, A. Gabay, G. Hadjipanayis, B. Balasubramanian, D. Sellmyer, Current progress and future challenges in rare-earth-free permanent magnets, Acta Mater. 158 (2018) 118–137.
[13] D. Goll, R. Loeffler, J. Herbst, R. Karimi, G. Schneider, High-throughput search for new permanent magnet materials, J. Phys. Condens. Matter. 26 (2014), 064208.
[14] Z. Li, A. Kedous-Lebouc, J.M. Dubus, L. Garbuio, S. Personnaz, Direct reuse strategies of rare earth permanent magnets for PM electrical machines-an overview study, EPJ Appl. Phys. 86 (2019) 20901.
[15] A. Lixandru, P. Venkatesan, C. Jönsson, I. Poenaru, B. Hall, Y. Yang, A. Walton, K. Güth, R. Gauß, O. Gutfleisch, Identification and recovery of rare-earth permanent magnets from waste electrical and electronic equipment, Waste Manag. 68 (2017) 482–489.
[16] J.R. Peeters, E. Bracqguene, D. Nelen, M. Ueberschaar, K. Van Acker, J.R. Duflou, Forecasting the recycling potential based on waste analysis: a case study for recycling Nd-Fe-B magnets from hard disk drives, J. Clean. Prod. 175 (2018) 96–108.
[17] U. Rösel, D. Drummer, Possibilities in recycling magnetic materials in applications of polymer-bonded magnets, Magnetism 2 (2022) 251–270.
[18] M. Grohol, C. Veeh, European Commission, Directorate-General for Internal Market, Industry, Entrepreneurship, SMEs. Study on the critical raw materials for the EU 2023 – Final report, Publications Office of the European Union, 2023. https://data.europa.eu/doi/10.2873/725585.
[19] S. Mandal, M. Debata, P. Sengupta, S. Basu, $L1_0$ FeNi: a promising material for next generation permanent magnets, Crit. Rev. Solid State Mater. Sci. (2022).
[20] A. Palomino, J. Marty, S. Auffret, I. Joumard, R.C. Sousa, I.L. Prejbeanu, B. Ageron, B. Dieny, Evaluating critical metals contained in spintronic memory with a particular focus on Pt substitution for improved sustainability, Sustain. Mater. Technol. 28 (2021) e00270.
[21] J. Li, S. Sharma, J. Li, S. Sharma, X. Liu, Y. Pan, J.S. Spendelow, M. Chi, Y. Jia, P. Zhang, D.A. Cullen, Z. Xi, H. Lin, Z. Yin, B. Shen, M. Muzzio, C. Yu, Y.S. Kim, A. A. Peterson, K.L. More, H. Zhu, S. Sun, Hard-magnet $L1_0$-CoPt nanoparticles advance fuel cell catalysis, Joule 3 (2019) 124–135.
[22] J. Li, Z. Xi, Y. Pan, J.S. Spendelow, P.N. Duchesne, D. Su, Q. Li, C. Yu, Z. Yin, B. Shen, Y.S. Kim, P. Zhang, S. Sun, Fe stabilization by intermetallic $L1_0$-FePt and Pt catalysis enhancement in $L1_0$-FePt/Pt nanoparticles for efficient oxygen reduction reaction in fuel cells, J. Am. Chem. Soc. 140 (2018) 2926.
[23] S. Sharma, C. Zeng, A.A. Peterson, Face-centered tetragonal (FCT) Fe and Co alloys of Pt as catalysts for the oxygen reduction reaction (ORR): a DFT study, J. Chem. Phys. 150 (2019), 041704.
[24] G. Varvaro, E. Agostinelli, S. Laureti, A.M. Testa, J.M. García-Martin, F. Briones, D. Fiorani, Magnetic anisotropy and intergrain interactions in $L1_0$ CoPt(111)/Pt (111)/MgO(100) PLD granular films with tilted easy axes, J. Phys. D. Appl. Phys. 41 (2008), 134017 (1–5).
[25] T. Speliotis, G. Varvaro, A.M. Testa, G. Giannopoulos, E. Agostinelli, W. Li, G. Hadjipanayis, D. Niarchos, Microstructure and magnetic properties of (001) textured $L1_0$ FePt films on amorphous glass substrate, Appl. Surf. Sci. 337 (2015) 118–124.
[26] T. Shima, K. Takanashi, Y.K. Takahashi, K. Hono, Preparation and magnetic properties of highly coercive FePt films, Appl. Phys. Lett. 81 (2002) 1050–1052.
[27] N. Bordeaux, A.M. Montes-arango, J. Liu, K. Barmak, L.H. Lewis, Thermodynamic and kinetic parameters of the chemical order–disorder transformation in $L1_0$ FeNi (tetrataenite), Acta Mater. 103 (2016) 608–615.

[28] G. Varvaro, P. Imperatori, S. Laureti, C. Cannas, A. Ardu, P. Plescia, A. Capobianchi, Synthesis of $L1_0$ alloy nanoparticles. Potential and versatility of the pre-ordered Precursor Reduction strategy, J. Alloy. Compd. 846 (2020), 156156.
[29] E. Poirier, F.E. Pinkerton, R. Kubic, R.K. Mishra, N. Bordeaux, A. Mubarok, L. H. Lewis, J.I. Goldstein, R. Skomski, K. Barmak, Intrinsic magnetic properties of $L1_0$ FeNi obtained from meteorite NWA 6259, J. Appl. Phys. 117 (2015) 17E318.
[30] L. Néel, J. Pauleve, R. Pauthenet, J. Laugier, D. Dautreppe, Magnetic properties of an iron-nickel single crystal ordered by neutron bombardment, J. Appl. Phys. 35 (1964) 873–876.
[31] E. Lima, V. Drago, A new process to produce ordered $Fe_{50}Ni_{50}$ tetrataenite, Phys. Status Solidi Appl. Res. 187 (2001) 119–124.
[32] A. Makino, P. Sharma, K. Sato, A. Takeuchi, Y. Zhang, K. Takenaka, Artificially produced rare-earth free cosmic magnet, Sci. Rep. 5 (2015) 16627.
[33] T. Kojima, M. Ogiwara, M. Mizuguchi, M. Kotsugi, T. Koganezawa, T. Ohtsuki, T. Y. Tashiro, K. Takanashi, Fe-Ni composition dependence of magnetic anisotropy in artificially fabricated $L1_0$-ordered FeNi films, J. Phys. Condens. Matter. 26 (2014), 064207 (1–10).
[34] K. Takanashi, M. Mizuguchi, T. Kojima, T. Tashiro, Fabrication and characterization of $L1_0$-ordered FeNi thin films, J. Phys. D. Appl. Phys. 50 (2017), 483002.
[35] S. Goto, H. Kura, E. Watanabe, Y. Hayashi, H. Yanagihara, Y. Shimada, M. Mizuguchi, K. Takanashi, E. Kita, Synthesis of single-phase $L1_0$-FeNi magnet powder by nitrogen insertion and topotactic extraction, Sci. Rep. 7 (2017) 13216.
[36] Y.P. Ivanov, B. Sarac, S.V. Ketov, J. Eckert, A.L. Greer, Direct formation of hard-magnetic tetrataenite in bulk alloy castings, Adv. Sci. 10 (2023), 2204315.
[37] S. Lee, K. Edalati, H. Iwaoka, Z. Horita, T. Ohtsuki, T. Ohkochi, M. Kotsugi, T. Kojima, M. Mizuguchi, K. Takanashi, Formation of FeNi with $L1_0$-ordered structure using high-pressure torsion, Philos. Mag. Lett. 94 (2014) 639–646.
[38] M. Gong, S. Ren, Phase transformation-driven surface reconstruction of FeNi nanostructures, Chem. Mater. 27 (2015) 7795–7800.
[39] G. Giannopoulos, G. Barucca, A. Kaidatzis, V. Psycharis, R. Salikhov, M. Farle, E. Koutsouflakis, D. Niarchos, A. Mehta, M. Scuderi, G. Nicotra, C. Spinella, S. Laureti, G. Varvaro, $L1_0$-FeNi films on Au-Cu-Ni buffer-layer: a high-throughput combinatorial study, Sci. Rep. 8 (2018) 15919.
[40] N. Maât, I. McDonald, R. Barua, B. Lejeune, X. Zhang, G.M. Stephen, A. Fisher, D. Heiman, I.V. Soldatov, R. Schäfer, L.H. Lewis, Creating, probing and confirming tetragonality in bulk FeNi alloys, Acta Mater. 196 (2020) 776–789.
[41] X.C. Hu, A. Capobianchi, R. Gallagher, G.C. Hadjipanayis, Influence of ball milling and annealing conditions on the properties of $L1_0$ FePt nanoparticles fabricated by a new green chemical synthesis method, J. Appl. Phys. 115 (2014) 10–13.
[42] X.C. Hu, E. Agostinelli, C. Ni, G.C. Hadjipanayis, A. Capobianchi, A low temperature and solvent-free direct chemical synthesis of $L1_0$ FePt nanoparticles with size tailoring, Green Chem. 16 (2014) 2292–2297.
[43] B. Astinchap, R. Moradian, A. Ardu, C. Cannas, G. Varvaro, A. Capobianchi, Bifunctional FePt@MWCNTs/Ru nanoarchitectures : synthesis and characterization, Chem. Mater. 24 (2012) 3393–3400.
[44] M. Faustini, A. Capobianchi, G. Varvaro, D. Grosso, Highly controlled dip-coating deposition of fct FePt nanoparticles from layered salt precursor into nanostructured thin films: an easy way to tune magnetic and optical properties, Chem. Mater. 24 (2012) 1072–1079.
[45] A. Capobianchi, S. Laureti, D. Fiorani, S. Foglia, E. Palange, Direct synthesis of $L1_0$ FePt nanoparticles within carbon nanotubes by wet chemical procedure, J. Phys. D. Appl. Phys. 43 (2010), 474013.
[46] A. Capobianchi, M. Colapietro, D. Fiorani, S. Foglia, P. Imperatori, S. Laureti, E. Palange, General strategy for direct synthesis of $L1_0$ nanoparticle alloys from layered precursor: the case of FePt, Chem. Mater. 21 (2009) 2007–2009.
[47] A. Capobianchi, G. Varvaro, P. Imperatori, Direct synthesis of L10 FeNi and other metal alloys, Nanostructured Magnetic Materials Lab, 2022 patent pending (#102022000024852).
[48] M. Kotsugi, H. Maruyama, N. Ishimatsu, N. Kawamura, M. Suzuki, M. Mizumaki, K. Osaka, T. Matsumoto, T. Ohkochi, T. Ohtsuki, T. Kojima, M. Mizuguchi, K. Takanashi, Y. Watanabe, Structural, magnetic and electronic state characterization of $L1_0$-type ordered FeNi alloy extracted from a natural meteorite, J. Phys. Condens. Matter. 26 (2014), 064206.
[49] K. Mibu, T. Kojima, M. Mizuguchi, K. Takanashi, Local structure and magnetism of $L1_0$-type FeNi alloy films with perpendicular magnetic anisotropy studied through 57Fe nuclear probes, J. Phys. D. Appl. Phys. 48 (2015), 205002.
[50] D.L. Leslie-Pelecky, R.D. Rieke, Magnetic properties of nanostructured materials, Chem. Mater. 8 (1996) 1770–1783.
[51] L. Néel, Théorie du traînage magnétique des ferromagnétiques en grains fins avec application aux terres cuites, Ann. Geophys. 5 (1949) 99–136.
[52] M. Kotsugi, M. Mizuguchi, S. Sekiya, M. Mizumaki, T. Kojima, T. Nakamura, H. Osawa, K. Kodama, T. Ohtsuki, T. Ohkochi, K. Takanashi, Y. Watanabe, Origin of strong magnetic anisotropy in $L1_0$-FeNi probed by angular-dependent magnetic circular dichroism, J. Magn. Magn. Mater. 326 (2013) 235–239.
[53] A. Cebollada, R.F.C. Farrow, M.F. Toney, Structure and magnetic properties of chemically ordered magnetic binary alloys in thin film form, in: H.S. Nalwa (Ed.), Magn. Nanostrucutres, American Scientific Publishers, 2002, p. 93.